Heat transfer characteristics of turbulent boundary layer flames stabilized under a mixed-convective environment

Alankrit Srivastava, Saurav Kumar, and Ajay V. Singh
Indian Institute of Technology, Kanpur
Kanpur - 208016, Uttar Pradesh, India

1 Introduction

Turbulent boundary-layer flames occur in almost all unwanted fires and are prevalent in both wildland fires and urban fires [1,2]. The heat feedback from the flame provides the necessary energy to vaporize a given fuel, resulting in a self-sustained boundary layer diffusion flame [3]. Furthermore, practical turbulent fires occur under mixed-convection mode where both buoyancy and wind speed affect the structure of such fires [4]. Many efforts have been undertaken in the past to quantify the various flame heat flux components and examine their influence on the burning process. However, the available literature reveals the widely dispersed data along with other difficulties while accurately estimating the local heat fluxes, particularly under mixed-convective turbulent flow conditions. More recently, by using gas-phase temperature measurements closer to the wall surface, Singh et al. [5] developed a novel methodology for the highly accurate calculation of local mass loss rates and heat flux distribution for laminar boundary layer diffusion flame sustained over a condensed fuel surface. By applying energy balance at the fuel surface, convective and radiative heat fluxes were estimated in the pyrolysis region. This methodology was verified as the most accurate way to quantify heat flux distribution and was adopted in several other studies [2]. Since this methodology requires the values of local mass burning rates, Singh et al. [6] developed a theoretical model to determine the local mass loss rate for the flame stabilized over the condensed fuel surface. Following the pioneering work of Emmons et al. [7] and Reynolds analogy, the authors developed a correlation that relates the non-dimensional temperature gradient at the fuel surface with the local mass loss rate through some constant of proportionality, as indicated in Eqn. (1). Here, B is defined as the Spalding mass transfer number, k_w is gas-phase thermal conductivity calculated at wall temperature, c_p is the specific heat calculated at the adiabatic flame temperature of the chosen fuel, Pr is known as the Prandtl number, L is the length of the pyrolysis zone, $(\partial T^*/\partial y^*)_{y^*=0}$ represents the non-dimensional temperature gradient evaluated at the fuel surface, and $y^* = y/L$ stands for the non-dimensional distance in the vertical direction. In addition, T^* exhibit non-dimensionalized temperature value defined as $\left(T - T_{w,p}\right)/\left(T_{fl,ad} - T_{w,p}\right)$, where $T_{w,p}$ is the wall temperature in the pyrolysis zone, and $T_{fl,ad}$ is the adiabatic flame temperature of the fuel.

$$\dot{m}_f^{"} = \frac{Bk_w}{c_p L}(Pr)^{2/3}\left(\frac{\partial T^*}{\partial y^*}\right)_{y^*=0} \quad (1)$$

Correspondence to: ajayvs@iitk.ac.in

The current study focused on estimating heat fluxes and examining their influence on the burning behavior of turbulent mixed-convective boundary layer diffusion flames. Further, a non-dimensional parameter was defined that encapsulates the property of the fuel, resulting in a more generalized correlation. The experimental data of a sooty fuel (n-heptane) and lightly-sooting fuel (ethanol) were used to develop meaningful correlations applicable to both laminar and turbulent flow conditions.

2 Experimental setup

Experiments were performed using a laboratory-scale wind tunnel. The test setup was developed for studying wind-driven flames under turbulent flow conditions, as shown in Fig. 1. The fuel wick ($25\ cm \times 8\ cm \times 1.27\ cm$) was prepared according to the procedure suggested by Singh et al. [5] to limit the burning to the top surface. In addition, for reducing flow separation and bluff body effects, a thin metallic sheet ($40.64\ cm \times 7\ cm \times 0.1\ cm$) was placed before the fuel wick [8]. The entire assembly was placed over a high-precision load cell that monitored the overall mass loss of the fuel sample for the specified period. R-type fine-wire thermocouples of wire diameter 50 μm were used for temperature measurements at high spatial resolution using a traverse mechanism. A data acquisition card (NI 9214) was used to acquire, condition, and digitalize the voltage signals from the thermocouples, where the measurement was conducted at a sampling rate of 100 samples/second for 10 sec at the specific location. Due to the usage of fine-wire thermocouples, the conduction errors were negligible (<1%) for this study. Also, while accommodating the radiation correction based on the approach given by Singh et al. [5], the error in local temperature gradients was found to be considerably lower. Hence, thermocouple radiation error was not considered in this study.

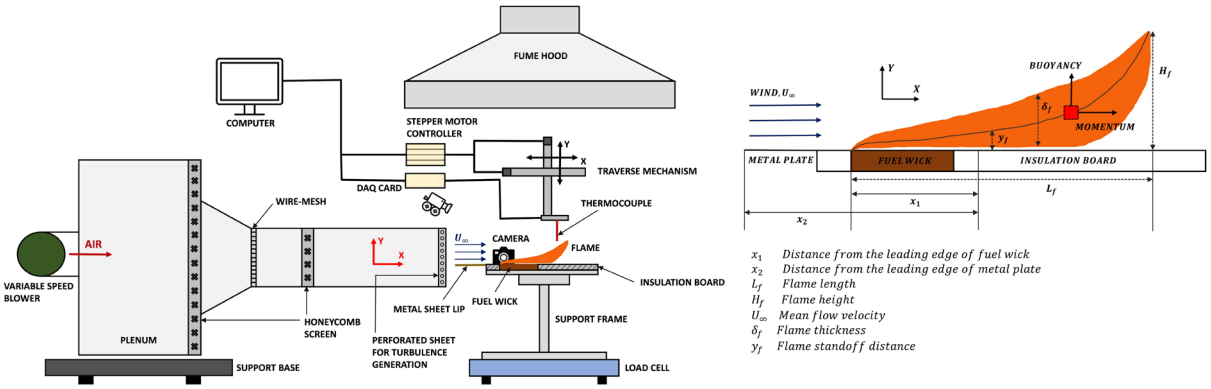

Fig. 1. Schematic of the experimental setup and structure of boundary layer diffusion flame.

Table 1. Turbulence grid details

Grid	Hole/Wire diameter	Center-to-center distance	Blockage ratio (BR)	Formula to evaluate blockage ratio
Grid 1	1.6 mm	3.2 mm	0.77	$1 - \frac{(\text{ hole diameter })^{2*}0.9089}{(\text{center-to-center distance })^2}$
Grid 2	3 mm	d_H = 6 mm d_V = 7 mm	0.83	$1 - \frac{(\text{ hole diameter })^{2*}0.785}{(d_H) * (d_V)}$
Wire Mesh	1.5 mm	14.7 mm	0.18	$1 - \frac{(\text{center-to-center distance})^2 * 1}{(\text{center-to-center distance } + \text{ wire diameter })^2}$

d_H – Horizontal distance, d_V – Vertical distance

Grid-based freestream turbulence was introduced in the flow path based on the work of Zhou et al. [1]. Various grids or wire mesh (Table 1) were installed at the exit section of the wind tunnel to obtain the

desired turbulence intensity. Flow characterization was performed with the help of a constant temperature hot-wire anemometer (CTA), where the data for average flow velocity and turbulence intensity was recorded at the leading edge of the fuel surface. While maintaining the dwell time of 60 seconds, the measurements were recorded (50,000 samples/sec) by traversing the hot-wire anemometer normal to the fuel surface, as shown in Fig. 2. The turbulence intensity (TI) can be expressed as $TI = u'/U_\infty$, where u' and U_∞ is defined as the root mean square (RMS) of velocity fluctuations and average flow velocity, respectively. The current study considered the crossflow velocity and turbulent intensity variation from 1 m/s to 1.8 m/s and 3% to 9%, respectively. Also, a Nikon D7000 digital camera was used to record side videos of the flame which were further processed in an image processing algorithm developed in MATLAB, as performed by Singh et al. [2]. Each experiment was repeated at least five times, and the overall uncertainty associated with velocity, load cell data, temperature, and flame parameter measurements, was found to be less than 3%, 2%, 4%, and 2.5%, respectively.

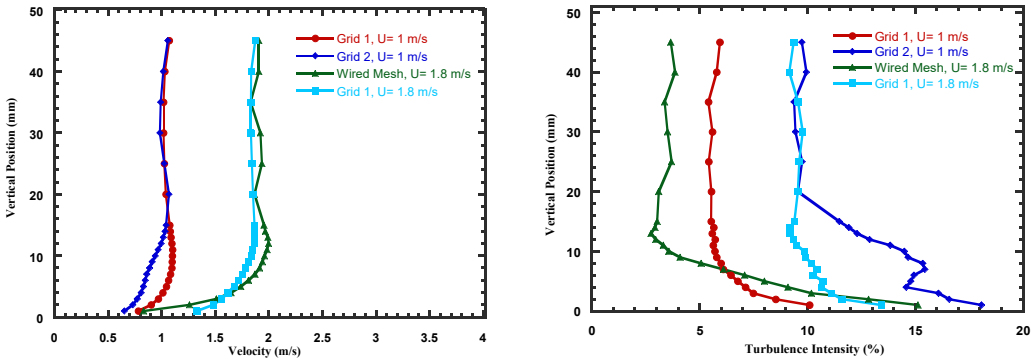

Fig. 2. Velocity and turbulence intensity profile at the leading edge of fuel wick.

3 Mixed-convective parameter

Buoyancy plays a vital role in the turbulent boundary layer diffusion flames sustained under a mixed-convection regime, particularly at low speeds. As an effect, the flame is uplifted from the fuel surface, reducing heat transfer to the surface. In contrast, momentum forces assist in keeping the flame closer to the fuel surface. A representation of these forces and flame parameters is shown in Fig. 1. Following the early works of Zhou et al. [1], a local forced-flow variable (ψ_{x_2}) was defined to account for both momentum and turbulence, as presented in Eqn. (2). Here, u'/U_∞ represent the turbulent intensity and v_f is the kinematic viscosity of air at mean film temperature. The mean film temperature (T_f) is calculated as $T_f = (T_{fl,ad} + T_w)/2$, where $T_{fl,ad}, T_w$ represents the fuel adiabatic flame temperature and wall surface temperature, respectively. Here, 'a' is the constant dependent on the fuel properties and orientation of the fuel surface.

$$\psi_{x_2} = \mathrm{Re}_{x_2}^{1/2}\left(1 + a(u'/U_\infty)^{1/2}\right) = \left(\frac{U_\infty x_2}{v_f}\right)^{1/2}\left(1 + a(u'/U_\infty)^{1/2}\right) \quad (2)$$

More recently, Singh et al. [2] also used a similar flow variable that considered the value of a = 0.47 for ethanol fuel, obtaining the best empirical fit that yields some important correlations. However, there is a need for a generalized correlation that would work for any particular fuel using some fuel property. Thus, to incorporate the chemical characteristic of the fuel, the constant 'a' was expressed as a function of mass transfer number (B), as represented in Eqn. (3). Also, a local Grashof number (Gr_{x_1}) was introduced to account for buoyancy effects in the flame, as represented by Eqn. (4). Here, β_f is the coefficient of thermal expansion calculated at the mean film temperature $(\beta_f = 1/T_f)$ and g is the acceleration due to gravity. Further, the combined influence of buoyancy, momentum, and turbulence can be represented in the form of a non-dimensional variable (ξ_x) as given in Eqn. (5). The proposed

correlation can be used for a given fuel, along with both laminar as well as turbulent crossflow conditions. The exponent 'n' values utilized in most studies are 3, 4, and 5, and similar values were also employed in this investigation. In this regard, for characterizing heat fluxes, the best empirical fit was obtained for the calculated value of $a = 0.577$ for n-heptane and $a = 0.458$ for ethanol [9], along with a value of $n = 3$.

$$a = \frac{\ln(1+B)}{2.6\,B^{0.15}} \tag{3}$$

$$\mathrm{Gr}_{x_1} = \frac{g\beta_f(T_{fl,ad}-T_w)x_1^3}{\nu_f^2} \tag{4}$$

$$\xi_x = Gr_{x_1}/\psi_{x_2}^n \tag{5}$$

4 Quantification of local heat fluxes in the pyrolysis zone

Following the methodology of Singh et al. [5], an energy balance can be made over the fuel surface, as presented in Eqn. (6-7). Here, $\dot{m}_f''$ represents local mass burning rate, L_v *is* the latent heat of vaporization of the fuel and $\dot{q}_{fl,c}''$, $\dot{q}_{fl,r}''$, $\dot{q}_{s,rr}''$ represent convective, radiative, & re-radiative heat fluxes, respectively. Also, k_w is the gas-phase thermal conductivity calculated at wall surface temperature (T_w), T_∞ is freestream temperature, and σ is known as the Stefan-Boltzmann constant.

$$\dot{m}_f'' L_v = \dot{q}_{fl,c}'' + \dot{q}_{fl,r}'' - \dot{q}_{s,rr}'' \tag{6}$$

$$\dot{m}_f'' L_v = k_w \left(\frac{\partial T}{\partial y}\right)_{y=0} + \dot{q}_{fl,r}'' - \sigma(T_w^4 - T_\infty^4) \tag{7}$$

Gas-phase temperature readings and local fuel loss rates along the condensed fuel surface are used to determine heat fluxes in the pyrolysis zone. Local temperature gradients at each *x*-location were used to compute the local convective heat flux. Further, average heat flux was evaluated by averaging local heat fluxes over the entire length of the fuel surface (80 mm). Using Eqn. (1), the local mass burning rate was calculated at each downstream position as presented in Table (2). Also, the variation of local mass loss rates over the entire fuel wick length was used to compute the average mass burning rate, which showed a good agreement with load cell data with less than 20% error.

Table 2. Verification of local mass burning rate model presented in Eqn. (1) for both fuels under different turbulent crossflow conditions.

Flow Conditions	**Load Cell (*g/m²s*)**	**Theoretical Correlation (Eqn. (1)) (*g/m²s*)**	**Error (%)**
n-Heptane			
U_∞ = 1 m/s, TI = 5%	27.87	31.33	12.41
U_∞ = 1 m/s, TI = 9%	28.57	31.86	11.52
U_∞ = 1.8 m/s, TI = 3%	32.93	32.19	-2.25
U_∞ = 1.8 m/s, TI = 9%	37.86	40.09	5.89
Ethanol			
U_∞ = 1 m/s, TI = 5%	14.20	14.94	5.25
U_∞ = 1 m/s, TI = 9%	14.26	14.66	2.80
U_∞ = 1.8 m/s, TI = 3%	15.26	16.65	9.14
U_∞ = 1.8 m/s, TI = 9%	15.98	19.05	19.21

Table 3 summarizes different heat flux components for n-heptane (sooty) and ethanol (low sooty) fuel. It was observed that the total incident heat flux ($\overline{\dot{q}_{s,i}''}$) increases with an increase in crossflow velocity. This is linked to the reduction of the flame standoff distance at higher velocities, which was also reported in other studies [2]. Also, the convective heat flux toward the fuel surface increases due to larger velocity

and temperature gradients at the wall surface for higher turbulence intensity flows. Further, it was observed that radiative flux dominates over the convective part for sooty fuel (n-heptane). In contrast, for ethanol (low sooty fuel), the contribution of convective heat flux plays a major role in overall heat flux falling on the virgin fuel surface. This is due to the presence of high soot content in the heptane flame, resulting in an enhanced radiative heat flux component. Additionally, a non-dimensional form of heat flux was defined to study its variation with other parameters. The corresponding heat flux component was divided by the term $\rho_\infty c_{p,\infty}(T_{fl,ad} - T_\infty)\sqrt{Agx_1}$ to obtain the non-dimensional form of total and convective heat flux. Here, $\rho_\infty, c_{p,\infty}$ represents the density & specific heat of air at ambient conditions, and $T_{fl,ad}$ is the adiabatic flame temperature of the chosen fuel. The term $\sqrt{Agx_1}$ signifies buoyant velocity, where A stands for Atwood number, which is defined as the difference between ambient and flame density values, $(\rho_\infty - \rho_{fl,ad})/(\rho_\infty + \rho_{fl,ad})$. As discussed earlier, both buoyancy and momentum influence the burning behavior and flame structure. Hence, heat flux can also be characterized using a mixed-convection parameter (ξ_x). In this regard, non-dimensional convective heat flux was plotted against the defined variable ξ_x, as shown in Fig. 3 (a). The heat flux data for both heptane and ethanol fuel were included, which showed a similar trend for both fuels. The following trendline was obtained while plotting the variation between non-dimensional heat flux and the defined parameter (ξ_x),

$$q^*_{fl,c} = 0.009(\xi_x)^{-0.321} \tag{8}$$

Table 3. Heat flux components at the fuel surface in the pyrolysis zone.

Crossflow Conditions	$\overline{\dot{q}''_{s,i}} = \overline{\dot{q}''_{fl,c}} + \overline{\dot{q}''_{fl,r}}$ *(kW/m²)*	$\overline{\dot{q}''_{fl,c}}$ *(kW/m²)*	$\overline{\dot{q}''_{fl,r}}$ *(kW/m²)*	$\overline{\dot{q}''_{fl,rr}}$ *(kW/m²)*	$\overline{\dot{q}''_{fl,c}}$ *(%)*
n-Heptane					
U_∞ = *1 m/s, TI = 5%*	40.34	13.29	27.05	22.11	31.25
U_∞ = *1 m/s, TI = 9%*	32.38	13.75	18.63	18.87	40.59
U_∞ = *1.8 m/s, TI = 3%*	41.37	14.07	27.30	23.70	33.01
U_∞ = *1.8 m/s, TI = 9%*	41.22	16.80	24.42	19.23	38.90
Ethanol					
U_∞ = *1 m/s, TI = 5%*	20.23	12.77	7.47	5.34	59.49
U_∞ = *1 m/s, TI = 9%*	19.11	12.98	6.13	5.29	65.08
U_∞ = *1.8 m/s, TI = 3%*	24.35	14.80	9.55	8.20	57.14
U_∞ = *1.8 m/s, TI = 9%*	22.44	16.76	5.68	3.97	71.02

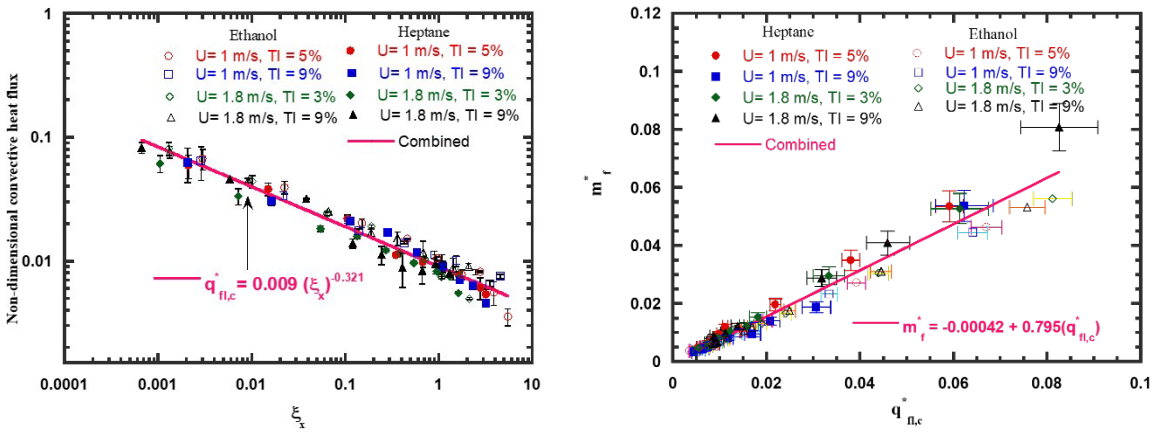

(a) (b)

Fig. 3. (a) Non-dimensional convective heat flux variation with ξ_x. (b) Non-dimensional mass burning rate (m^*_f) variation with dimensionless convective heat flux ($q^*_{fl,c}$).

Further, to observe the interdependence of mass burning rate with heat flux, a non-dimensional form of local mass burning rate was defined by dividing the product of mass transfer number (B) and buoyant mass flux ($\dot{m}_b''$), as stated in Eqn. (9). A dimensionless form of the local mass loss rate was plotted against the non-dimensional convective heat flux ($q_{fl,c}^*$), as shown in Fig. 3 (b). It was observed that a direct proportionality existed between the non-dimensional form of mass loss rate and convective heat flux. In this regard, a power-law fit was obtained by fitting the non-dimensional local mass burning rate with dimensionless convective heat flux as represented in Eqn. (10).

$$m_f^* = \dot{m}_f''/B\,\dot{m}_b'' = \dot{m}_f''/B\rho_\infty\sqrt{Agx_1} \tag{9}$$

$$m_f^* = -0.00042 + 0.795\left(q_{fl,c}^*\right) \tag{10}$$

5 Conclusions

The current study quantifies the convective and radiative components of flame heat flux in the pyrolysis zone using the data of local mass burning rates and temperature gradients. The experimental data of two fuels (n-heptane and ethanol) was analyzed, and meaningful correlations were developed for turbulent wind-driven flames stabilized under a mixed-convective environment. In most situations, both fuels showed similar trends; however, for n-heptane, the radiative heat flux was found to be dominant due to the presence of a high amount of soot. To characterize flame-burning behavior under the combined influence of momentum, buoyancy, and flow turbulence, a local mixed-convection parameter (ξ_x) was defined in the form of $Gr_{x_1}/\psi_{x_2}^n$, where Gr_{x_1} is Grashof number and ψ_{x_2} is a turbulent forced-flow variable. The interdependence of heat flux parameters with mass burning rate and the mixed-convective parameter helped us understand the combustion characteristics of wind-driven flames and provide meaningful correlations.

References

[1] L. Zhou, Concurrent Turbulent Flame Spread, Symposium (International) on Combustion. 23 (1991) 1709–1714.

[2] A. Singh, A. V. Singh, Burning behavior of mixed-convection wind-driven flames under varying freestream conditions, Fire Saf J. 122 (2021) 103320.

[3] A.C. Fernandez-Pello, T. Hirano, Controlling mechanisms of flame spread, Combustion Science and Technology. 32 (1983) 1–31.

[4] C.H. Miller, W. Tang, E. Sluder, M.A. Finney, S.S. McAllister, J.M. Forthofer, M.J. Gollner, Boundary layer instabilities in mixed convection and diffusion flames with an unheated starting length, Int J Heat Mass Transf. 118 (2018) 1243–1256.

[5] A. V. Singh, M.J. Gollner, A methodology for estimation of local heat fluxes in steady laminar boundary layer diffusion flames, Combust Flame. 162 (2015) 2214–2230.

[6] A. V. Singh, M.J. Gollner, Estimation of local mass burning rates for steady laminar boundary layer diffusion flames, Proceedings of the Combustion Institute. 35 (2015) 2527–2534.

[7] H.W. Emmons, The Film Combustion of Liquid Fuel, Journal of Applied Mathematics and Mechanics. 36 (1956) 60–71.

[8] J.S. Ha, S.H. Shim, H.D. Shin, Boundary layer diffusion flame over a flat plate in the presence and absence of flow separation, Combustion Science and Technology. 75 (1991) 241–260.

[9] J.G. Quintiere, Fundamentals of Fire Phenomena, 2006.